

Shock waves and population inversion in collisions of ultracold atomic clouds

Sebastiano Peotta^{1,*} and Massimiliano Di Ventra¹

¹*Department of Physics, University of California-San Diego, La Jolla, CA 92093, USA*

Ultracold atomic gases represent an ideal toolbox to study quantum effects that are difficult to probe using other systems. Here, we use a time-dependent density matrix renormalization group approach to show that the collision of two interacting bosonic clouds in one dimension gives rise to shock waves with a concomitant local energy distribution typical of population inversion, *i.e.*, an effective negative temperature. A classical hydrodynamic description compares well with the exact quantum dynamics only up to the gradient catastrophe time. Such a highly nonequilibrium local distribution, however, does not prevent the system from recovering its initial state after an oscillation period which is renormalized by the interaction. All these results can be easily tested experimentally.

PACS numbers: 67.10.Jn, 67.85.Lm

Experiments on ultracold atomic gases have unveiled new aspects of quantum systems comprising a large number of particles, *i.e.*, of quantum fields. The degree of isolation from the external environment and the long time scales allow to study details of the quantum dynamics that are not easily accessible, *e.g.*, in solid-state systems. Moreover, the dynamics are often nonlinear and a substantial effort is needed to restrict the system to a regime where linear response theory is applicable [1]. As a consequence, the concept of quasiparticle – an elementary excitation above the ground state – is hardly of any help in understanding the time evolution. Instead, at very low temperatures the system behaves rather as a single *collective* object, and a description in terms of fields rather than point particles is more appropriate.

Examples of collective quantum dynamics are collision experiments between clouds of ultracold atomic gases. Various phenomena have been studied in this context such as the interference of matter waves [2], dispersive shock-waves in BECs [3, 4], superfluidity, shock-wave formation and domain wall propagation in the unitary Fermi gas [5, 6], spin transport [7], and lack of thermalization in quasi-integrable 1D systems [8, 9]. Most recently [10] a *negative temperature*, namely a *population inversion* in the energy distribution of the motional degrees of freedom of atomic gases at equilibrium has been realized. In this work it was also noted that such a population inversion does not necessarily imply a fast decay to the true thermal equilibrium state, thus showing the quite unique properties these systems possess.

In this Letter we show that out of equilibrium distributions characterized by an effective negative temperature have also been realized in the “quantum Newton cradle” of Ref. [8] for almost any value of the interaction strength. With reference to this experimental set up, we study the collision of two clouds of one dimensional bosons for arbitrary interaction strength, by means of a time-dependent density matrix renormalization group (TDMRG) approach [11–14]. We demonstrate both the emergence of population inversion (negative ef-

fective temperature) at the onset of shock waves – where a hydrodynamic description deviates from the exact quantum dynamics – and no visible decay in the density profile or in the local energy distribution function as a function of time, despite the presence of population inversion. Instead, the dynamics are essentially periodic with the oscillation frequency renormalized by the interaction strength. All these results can be easily verified experimentally.

Model and methods — The Lieb-Liniger model [15, 16] provides an excellent description of one-dimensional ultracold bosonic atoms [17, 18]. In terms of a bosonic field $\hat{\Psi}(x)$ its Hamiltonian reads

$$\hat{\mathcal{H}}_{\text{LL}} = \int dx \left[\frac{\hbar^2}{2m} |\partial_x \hat{\Psi}(x)|^2 + \frac{g_B}{2} |\hat{\Psi}(x)|^4 + V(x) |\hat{\Psi}(x)|^2 \right], \quad (1)$$

where $g_B \in [0, +\infty]$ is a coupling constant and m is the atom mass. In the following we will consider a time-dependent external potential $V(x, t)$ changing abruptly at $t = 0$ (*quench protocol*). Hamiltonian (1) is integrable for any g_B when $V(x) = 0$, while for $V(x) \neq 0$ the exact eigenstates and eigenvalues are known for free bosons $g_B = 0$ and hardcore bosons $g_B = +\infty$, the latter being equivalent to free fermions (Bose-Fermi mapping theorem [19, 20]).

In the following we consider a closed finite system of $N = 20$ particles [21] initially prepared in the ground state of a double well potential of the form

$$V(x, t = 0) = \frac{1}{2} m \omega_1 \frac{(x^2 - D^2)^2}{4D^2}. \quad (2)$$

At subsequent times $t > 0$ the trapping potential becomes

$$V(x, t > 0) = \frac{1}{2} m \omega_2 x^2. \quad (3)$$

and the two clouds are forced to collide (*microcanonical picture of transport* [22, 23]).

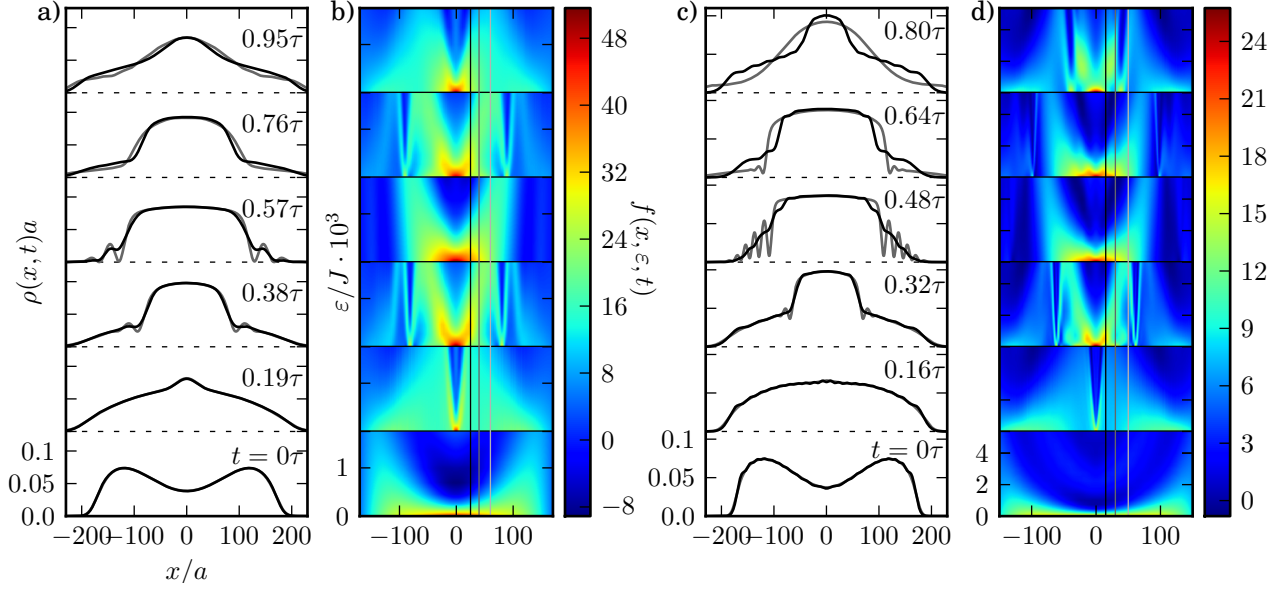


FIG. 1. (Color online) **a)** Snapshots of the density profile $\rho(x,t)$ in units of $1/a$ at various times for $g_B = 0.2J/a$ ($\gamma = 2$). The black lines are the exact TDRMG results, the grey lines are obtained from the solution of Eq. (4). At $t = 0$ the two profiles are indistinguishable, but they deviate from each other at the onset of shock-wave formation ($t = 0.38\tau$). **b)** Energy distribution function $f(x,\varepsilon,t)$ (6) calculated from the exact Wigner function (5) obtained with TDRMG. The color plots show the values of $f(x,\varepsilon,t)$ in the (x,ε) plane at the corresponding times in panel a). The vertical black, grey and light grey lines correspond to the sections for fixed x of $f(x,\varepsilon,t)$ shown in Fig. 2. Note that shock-wave formation is characterized by a highly nonequilibrium distribution. **c)-d)** Same as panels a) and b) but for $g_B = 2.0J/a$ ($\gamma = 20$). The shock-wave for $g_B = 2.0J/a$ forms at roughly the same time $t = 0.32\tau$ as for $g_B = 0.2J/a$.

We are able to access the *exact* dynamics of (1), (2) and (3) with a TDRMG approach. TDRMG has been applied mainly to lattice systems for relatively short time scales, but simulations of systems in the continuum limit and for quite long time scales (of the order of several trapping potential periods) are feasible [26–30]. In our simulations we have employed two different discretizations of (1) [26, 31], either as a Bose-Hubbard model (nonintegrable), or as a XXZ spin chain (integrable) using the Bose-Fermi mapping for arbitrary g_B [24–26]. No substantial difference in the results has been observed.

In the following, lengths are expressed in units of the lattice spacing a of the discretized model, which is a small, but otherwise arbitrary length scale, energy is in units of $J = \hbar^2/(2ma^2)$, and time in units of the post-quench oscillation period $\tau = \pi/\omega_2$. The interaction parameter g_B is given in units of J/a . Occasionally we use the Lieb-Liniger parameter $\gamma = mg_B/(\hbar^2\rho)$ with $\rho = 0.05/a$, an indicative value of the density in the inhomogeneous system considered here. In our simulation we used a lattice of length $L = 600a$ and $D = 120a$ [see (2)]. We ensured, by separately tuning ω_1 and ω_2 for each value of the coupling g_B , that the particle density *per site* never exceeds 0.15, thus lattice effects are negligible (continuum limit) [28, 29, 31].

Numerical results and hydrodynamic description — TDRMG is based on the *matrix product state* repre-

sentation of the full wave function [14]. However the Runge-Gross theorem [32] of Time-Dependent Density Functional Theory (TD-DFT) guarantees that an exact hydrodynamic description (purely in terms of density and velocity fields) of quantum dynamics exists [22], although the analytical expression of the stress tensor is unknown even for free fermions [33, 34]. To our knowledge the best possible hydrodynamic description for the present case is a generalized nonlinear Schrödinger equation (GNLSE) [18, 35–38]

$$i\hbar\partial_t\Psi(x,t) = -\frac{\hbar^2}{2m}\partial_x^2\Psi(x,t) + \phi(\rho)\Psi(x,t) + V(x,t)\Psi(x,t), \quad (4)$$

where $\Psi(x)$ is a complex field, $V(x,t)$ is specified by (2) and (3), $\rho(x) = |\Psi(x)|^2$ is the density, and $\phi(\rho)$ the Gibbs free energy per particle which can be obtained in the local density approximation (LDA) from the Bethe Ansatz solution of the Lieb-Liniger model. Accurate numerical values of this quantity are available [18]. We employ this hydrodynamic description to better identify the time of formation of shock waves.

TDRMG and hydrodynamics are compared in Fig. 1 for $g_B = 0.2J/a$ and $g_B = 2.0J/a$. The excellent agreement for $t = 0$ indicates that lattice effects are negligible (continuum limit) and that LDA works well for just $N = 20$ particles. The hydrodynamic description is seen to model well the dynamics of the density immediately

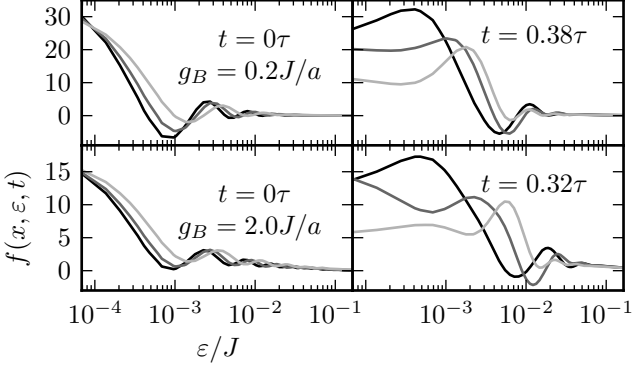


FIG. 2. Energy distribution function $f(x, \varepsilon, t)$ corresponding to first ($t = 0\tau$) and third ($t \sim 0.3\tau$) snapshots in Fig. 1, panels b) and d). The black, grey and light grey lines correspond to $x/a = 25, 40, 60$ for the two upper quadrants ($g_B = 0.2J/a$) [Fig. 1 panel b)], and $x/a = 15, 30, 50$ for the two lower quadrants ($g_B = 2.0J/a$) [Fig. 1 panel d)], respectively. Note that, neglecting oscillations for large ε – due to the finite number of particles – the initial distribution decreases monotonically, while a maximum develops for finite ε after the shock-wave formation $t \sim 0.3\tau$, *i.e.* a population inversion.

after the quench. However it fails when oscillations form in the GNLSE solution ($t = 0.38\tau$ Fig. 1a, $t = 0.32\tau$ Fig. 1c, grey lines), corresponding to the formation of shock waves (*gradient catastrophe* [39, 40]). These shock waves with oscillatory behaviour are known as *dispersive* and occur in inviscid fluids, e.g. Bose-Einstein condensates [3, 4, 40].

Our TDMRG results are very similar to the experimental data reported in Ref. 5 where a viscosity was introduced in the hydrodynamic equations to describe shock waves, while in the TD-DFT calculation in Ref. 41 a renormalized kinetic term $\lambda \partial_x^2 \Psi$ was used for the same reason. This is not justified here since Eq. (4) has no free parameters and it is an excellent approximation up to the gradient catastrophe for *any* g_B . Introducing viscosity would contradict the fact that almost no dissipation is present in our system (see below).

Population inversion and negative temperature — In order to study in more detail the particle distribution during the quantum shock wave, we use the Wigner function [33, 34]

$$W(x, p, t) = \frac{1}{\hbar\pi} \int dy \rho(x+y, x-y; t) e^{\frac{2ipy}{\hbar}}, \quad (5)$$

where $\rho(x', x; t) = \langle \hat{\Psi}^\dagger(x', t) \hat{\Psi}(x, t) \rangle$ is the one-body density matrix. The exact one-body density matrix is easily accessible within TDMRG. Neglecting negative values, $W(x, p, t)$ can be thought of as a local *momentum* (p) distribution as in the Boltzmann equation [43]. The local *energy* distribution $f(x, \varepsilon, t)$ is defined with respect to the local comoving (Lagrangian) reference

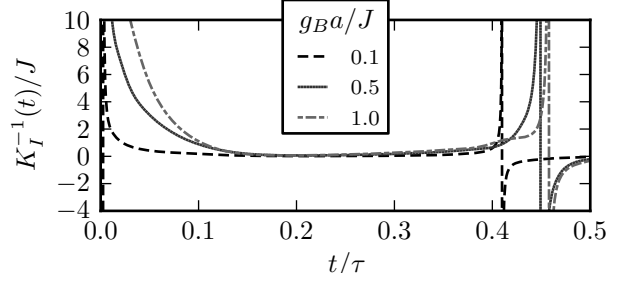


FIG. 3. Inverse information compressibility as a function of time for various interaction strengths $g_B a/J = 0.1, 0.5, 1.0$. Note the divergence in correspondence to a fully developed shock wave at $t = 0.4 \div 0.5\tau$. See Fig. 1, snapshots at $t = 0.38\tau$ in panel a) and at time $t = 0.32\tau$ in panel c).

frame with velocity $mv(x, t) = j(x, t)/\rho(x, t)$ [22], with $j(x) = \int dp p W(x, p, t)$ and $\rho(x, t) = \int dp W(x, p, t)$. Thus $\int dp W(x, p - mv(x), t) = 0$ and the energy distribution reads [42]

$$f(x, \varepsilon, t) = 2\pi\hbar \sum_{s=\pm} W(x, s\sqrt{2m\varepsilon} - mv(x)). \quad (6)$$

This is the quantity shown in the color plots in Fig. 1 and for selected values of x in Fig. 2. At $t = 0$ the distribution $f(x, \varepsilon, t)$ decreases monotonically with ε (leaving aside oscillations related to the finite particle number) indicating an equilibrium energy distribution. In correspondence of the shock-wave formation $t \sim 0.3\tau$ the energy distribution is no longer an equilibrium one, $f(x, \varepsilon, t)$ is larger for values of ε away from zero (see Fig. 1 and quadrants at the right of Fig. 2), signalling a population inversion, namely an effective negative temperature. Population inversion leads to the break down of the LDA, namely to the departure from the GNLSE (Eq. 4) solution. Notice also that we have observed nonequilibrium distributions during the evolution for $g_B \geq 0.02J/a$, a rather small value of the interaction parameter corresponding to an average Lieb-Liniger parameter of $\gamma = 0.2$, well within the weakly interacting regime, thus suggesting that such phenomena should be present at all interaction strengths.

In order to corroborate the presence of a negative temperature out of equilibrium we characterize the state of the system with the *information compressibility* [44], which measures the relative change of number of available microstates of an open system in response to an energy variation. Given a system with density matrix $\hat{\rho}(t)$ and Hamiltonian $\hat{\mathcal{H}}$, the energy is $E(t) = \text{Tr}[\hat{\rho}(t)\hat{\mathcal{H}}]$ and the thermodynamic entropy $S(t) = -k_B \text{Tr}[\hat{\rho}(t) \ln \hat{\rho}(t)]$. Call Ω the number of microstates available to the system. The information compressibility is defined as the relative variation of the number of microstates with re-

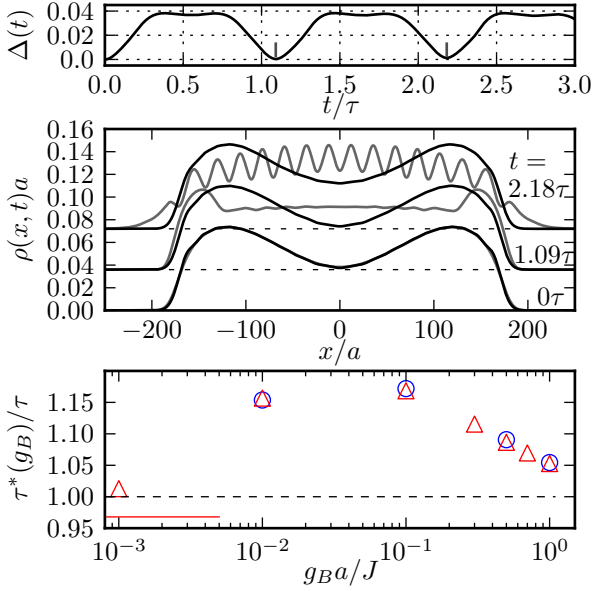


FIG. 4. (Color online) Upper plot, deviation $\Delta(t)$ as a function of time for $g_B = 0.5J/a$. The vertical notches indicate the instants ($t = 1.09\tau$ and 2.18τ) where the density is closest to the initial one. The corresponding density profiles are shown in the middle panel (black lines) along with the hydrodynamic results which do not show periodicity (grey). The density profiles at different times have been shifted in the vertical direction. In the lower plot the renormalized oscillation period $\tau^*(g_B)/\tau$ is shown, with $\tau = \pi/\omega_2$, as a function of the interaction strength g_B extracted from the minima of $\Delta(t)$ as in the upper plot. The red triangles show the results obtained with the XXZ spin chain discretization while the blue circles with the numerically more demanding Bose-Hubbard discretization. The red line at the bottom left represents the frequency extracted from the $g_B = 0$ exact data. It deviates from the exact result $\tau^*(0) = \tau$ since lattice effects distort the density profile in time [31]. This is not an error due to the approximation introduced by TDMRG.

spect to the energy variation at time t [44]

$$K_I(t) = \frac{1}{\Omega} \frac{\delta \Omega}{\delta E} \Big|_t. \quad (7)$$

Using the microcanonical relation $\Omega = \exp(S/k_B)$ one arrives at the computationally more convenient definition

$$K_I(t) = \frac{1}{k_B} \frac{\delta S}{\delta E} \Big|_t = \frac{1}{k_B} \frac{\partial S}{\partial t} \frac{\partial t}{\partial E} \Big|_t. \quad (8)$$

Note the similarity of this quantity with the thermodynamic definition of inverse temperature [44]. Here, we take for $\hat{\rho}(t)$ the density matrix of half of the system, *i.e.*, relative to the interval $[-L/2, 0]$. The results for the inverse information compressibility are shown in Fig. 4 for various interaction strengths. The interesting point is the divergence of $K_I^{-1}(t)$ in all cases for $t/\tau \sim 0.4$, *i.e.*, in correspondence to a fully-developed shock wave, and

negative values of this quantity at later times. If we interpret the inverse compressibility as an effective temperature, this behaviour is clearly suggestive of a population inversion, in agreement with our previous results.

Oscillation frequency shift — Finally, we note that although the system explores strongly nonequilibrium energy and momentum distributions we find that the initial density profile and the initial Wigner function are recovered after a time of order τ for any $g_B \in [0, +\infty]$. This periodicity is clearly seen in the mean square deviation of the density profile at time t from the initial one

$$\Delta(t) = \frac{1}{N} \sqrt{\int dx (n(x, t) - n(x, 0))^2}, \quad (9)$$

shown for $g_B = 0.5J/a$ in the upper panel of Fig. 4. $\Delta(t)$ essentially drops to zero at times $t = 1.09\tau$ and $t = 2.18\tau$ indicating that the system has returned to the initial state, at least within our simulation times. The density profiles corresponding to the minima of $\Delta(t)$ are shown in the middle panel of Fig. 4 alongside with the results of classical hydrodynamics. While the exact dynamics are essentially periodic, the classical one are not. We remind the reader that the static density (as shown in the lower $t = 0\tau$ profile in Fig. 4) and the dynamics up to the gradient catastrophe are well captured by the GNLSE (4). A similar analysis can be performed for all g_B and the renormalized period $\tau^*(g_B)$ is shown in the lower panel of Fig. 4. In the exactly solvable limits $g_B = 0$ and $g_B = +\infty$ the period is not renormalized. In between these extrema it has a nonmonotonic behaviour with a maximum in the interval $0.01 < g_B a/J < 0.1$ ($0.2 < \gamma < 2$). The almost perfect periodicity observed for any g_B is a strong indication of very small dissipation, in agreement with experimental results [8].

Conclusions — Using TDMRG we have computed the exact dynamics of interacting bosons in a 1D collision experiment for arbitrary interaction strengths, and compared the results with a parameter-free hydrodynamics deduced from the exact Bethe-Ansatz solution in the LDA. Even for small coupling, shock-wave formation leads to the break down of the hydrodynamic description. We have shown that quantum shock waves lead to a population inversion in the local energy distribution, namely to a negative effective temperature. Finally, we have computed the shift in the oscillation period due to interactions, a prediction which can be easily tested in experiments. Our results suggest that statistical ensembles with negative temperatures for the motional degrees of freedom, as shown in Ref. [10], are a common feature in collision experiments with ultracold gases [8].

This work has been supported by DOE under Grant No. DE-FG02-05ER46204. We thank C.-C. Chien for a critical reading of our paper.

* speotta@physics.ucsd.edu

- [1] M. Endres, T. Fukuhara, D. Pekker, M. Cheneau, P. Schauß, C. Gross, E. Demler, S. Kuhr, I. Bloch, *Nature* **487**, 454 (2012).
- [2] M. R. Andrews, C. G. Townsend, H.-J. Miesner, D. S. Durfee, D. M. Kurn, W. Ketterle *Science* **275**, 637 (1997).
- [3] M. A. Hoefer, M. J. Ablowitz, I. Coddington, E. A. Cornell, P. Engels, and V. Schweikhard, *Phys. Rev. A* **74**, 023623 (2006).
- [4] R. Meppelink, S. B. Koller, J. M. Vogels, and P. van der Straten, E. D. van Ooijen, N. R. Heckenberg, and H. Rubinsztein-Dunlop, S. A. Haine and M. J. Davis, *Phys. Rev. A* **80** 043606 (2009).
- [5] J. A. Joseph, J. E. Thomas, M. Kulkarni, A. G. Abanov, *Phys. Rev. Lett.* **106**, 150401 (2011).
- [6] Aurel Bulgac, Yuan-Lung Luo, Kenneth J. Roche, *Phys. Rev. Lett.* **108**, 150401 (2012).
- [7] A. Sommer, M. Ku, G. Roati, M. W. Zwierlein, *Nature* **472**, 201204 (2011).
- [8] T. Kinoshita, T. Wenger and David S. Weiss, *Nature* **440**, 900 (2006).
- [9] A. Polkovnikov, K. Sengupta, A. Silva, M. Vengalattore, *Rev. Mod. Phys.* **83**, 863 (2011).
- [10] S. Braun, J. P. Ronzheimer, M. Schreiber, S. S. Hodgman, T. Rom, I. Bloch, U. Schneider, *Science* **339**, 52 (2013).
- [11] S. R. White, A. E. Feiguin, *Phys. Rev. Lett.* **93**, 076401 (2004).
- [12] Guifré Vidal, *Phys. Rev. Lett.* **93**, 040502 (2004).
- [13] A. J. Daley, C. Kollath, U. Schollwöck and G. Vidal, *J. Stat. Mech.* (2004) P04005.
- [14] U. Schollwöck, *Ann. Phys. (NY)* **326**, 96 (2011).
- [15] E. H. Lieb, W. Liniger, *Phys. Rev.* **130**, 1605 (1963).
- [16] E. H. Lieb, *Phys. Rev.* **130**, 1616 (1963).
- [17] M. Olshanii, *Phys. Rev. Lett.* **81**, 938 (1998).
- [18] V. Dunjko, V. Lorent, M. Olshanii, *Phys. Rev. Lett.* **86**, 5413 (2001).
- [19] M. Girardeau, *J. Math. Phys.* **1**, 516 (1960).
- [20] M. Girardeau, *Phys. Rev.* **139**, 500 (1965).
- [21] The number of particles is irrelevant for our conclusions so long as $N \gg 1$. This has been verified in the easier case of free fermions where a scaling in the number of particles can be easily performed.
- [22] M. Di Ventra, *Electrical transport in nanoscale systems*, (Cambridge University Press, 2008).
- [23] C.-C. Chien, M. Zwolak and M. Di Ventra, *Phys. Rev. A* **85** 041601 (2012).
- [24] T. Cheon, T. Shigehara, *Phys. Rev. Lett.* **82** 2536 (1999).
- [25] T. Cheon, T. Shigehara, *Phys. Lett. A* **243**, 111 (1998).
- [26] D. Muth, M. Fleischhauer, B. Schmidt, *Phys. Rev. A* **82**, 013602 (2010).
- [27] D. Muth, *J. Stat. Mech.* (2011) P11020.
- [28] S. Peotta, D. Rossini, P. Silvi, G. Vignale, R. Fazio, and M. Polini, *Phys. Rev. Lett.* **108**, 245302 (2012).
- [29] S. Peotta, D. Rossini, M. Polini, F. Minardi, R. Fazio, *Phys. Rev. Lett.* **110**, 015302 (2013).
- [30] M. Knap, C. J. M. Mathy, M. B. Zvonarev, E. Demler, *arXiv:1303.3583*.
- [31] S. Peotta and M. Di Ventra, in preparation.
- [32] E. Runge, E. K. U. Gross, *Phys. Rev. Lett.* **52**, 997 (1984).
- [33] E. Bettelheim, L. Glazman, *Phys. Rev. Lett.* **109**, 260602 (2012).
- [34] I. V. Protopopov, D. B. Gutman, P. Schmitteckert, A. D. Mirlin, *arXiv:1209.1079*.
- [35] Y.E. Kim, A.L. Zubarev, *Phys. Rev. A* **67**, 015602 (2003).
- [36] B. Damski, *Phys. Rev. A* **69**, 043610 (2004).
- [37] B. Damski, *Phys. Rev. A* **73**, 043601 (2006).
- [38] We used a fourth order Trotter expansion to perform imaginary time evolution of Eq. (4) in the initial potential (2), thus providing the initial state $\Psi(x, t = 0)$. A sixth order Trotter expansion was used to evolve the system in the quenched potential (3). Exactly the same expansion has been employed for TDMRG simulations.
- [39] G. B. Whitham, *Linear and nonlinear waves*, Wiley (1974).
- [40] M. Kulkarni, A. G. Abanov, *Phys. Rev. A* **86**, 033614 (2012).
- [41] F. Ancilotto, L. Salasnich, F. Toigo, *Phys. Rev. A* **85**, 063612 (2012).
- [42] The energy distribution function in the usual sense is $\sqrt{m/(2\epsilon)}f(x, \epsilon, t)$ and contains the 1D density of states factor $\sqrt{m/(2\epsilon)}$. However, for our purposes the definition in Eq. (6) is more appropriate since for a classical system at equilibrium $f(x, \epsilon, t) \propto e^{-\beta\epsilon}$ and a monotonically increasing behaviour in the distribution directly corresponds to a negative temperature. This would not be immediately apparent if the 1D density of states had been taken into account. For quantum systems similar considerations hold.
- [43] Oscillations and negative values of the Wigner function obviously spoil its interpretation as a local momentum distribution. However, we have found in the case of free fermions, where a scaling with the number of particles is possible, that such features do not preclude a well defined Fermi step with increasing N [31].
- [44] M. Di Ventra and Y. Dubi, *Europ. Phys. Lett.* **85**, 40004 (2009).